JOURNAL OF Materials CHEMISTRY

Magnetic ordering in diluted kagome antiferromagnets†

Jan Frunzke,[a] Thomas Hansen,[b] Andrew Harrison,*[a] James S. Lord,[c] Gareth S. Oakley,[a] Dirk Visser[c,d,e] and Andrew S. Wills[a,f]

[a]*Department of Chemistry, The University of Edinburgh, Edinburgh, UK EH9 3JJ. E-mail: a.harrison@ed.ac.uk*
[b]*Institut Laue-Langevin, Avenue des Martyrs, BP 156, 38042 Grenoble Cédex 9, France*
[c]*The ISIS Facility, Rutherford Appleton Laboratory, Chilton, Didcot, Oxon, UK OX11 0QX*
[d]*Department of Physics, University of Warwick, Coventry, UK CV4 7AL*
[e]*IRI, TU Delft, Mekelweg 15, 2629 JB Delft, The Netherlands*
[f]*Département de Recherche Fondamentale sur la Matière Condensée, SPSMS, CEA Grenoble, 38054 Grenoble, France*

Received 17th May 2000, Accepted 12th June 2000
First published as an Advance Article on the web 12th October 2000

Potassium iron jarosite, $KFe_3(SO_4)_2(OH)_6$, provides a model kagome Heisenberg antiferromagnet with which to study the behaviour of this highly frustrated system. Magnetic susceptibility, powder neutron diffraction and muon spin relaxation measurements have been performed on samples of protonated and deuterated potassium iron jarosite in which some of the iron is replaced by aluminium ions to study the effect of diamagnetic dilution. The two successive magnetic ordering transitions of the pure material drop in temperature on doping. In all cases the low temperature phase appears to have long-range ordering of all moments in an array which is coplanar or nearly coplanar with the crystallographic *ab* axes, while in the intermediate phase there is a component of moment along the *c*-axis and some degree of dynamic character.

1 Introduction

One of the principal challenges in solid-state science today is to develop a better understanding of materials with strongly fluctuating ground states, and particularly those in which fluctuations between states of the same or similar energy may be coupled to another property such as charge transport to produce, for example, superconductivity.[1] One method of producing such multi-degenerate, or near-degenerate ground states is by geometrical frustration[2,3] which is illustrated for the case of a simple triangular tile in Fig. 1. In the case where magnetic exchange is antiferromagnetic, it is impossible to decorate the tile with moments so that they are simultaneously parallel to both neighbours (Fig. 1(a)); the compromise arrangements of lowest energy are depicted in Fig. 1(b) and (c), which differ only in the handedness, or 'chirality' of spins around the triangle. When these tiles are connected to produce a lattice in two dimensions, the degeneracy will depend upon the connectivity of the lattice. Fig. 2 depicts the so-called kagome lattice in which the triangular tiles are connected through vertices, and when this is decorated with antiferromagnetically coupled moments there are many degenerate ways of arranging them. Theory indicates[4–10] that even when the moments are free to possess components along *x*, *y* or *z* (where the *x*–*y* plane is the plane of the paper in these Figures), they chose to adopt a co-planar array, and Fig. 2(a) and (b) depict two degenerate co-planar arrays, respectively called the $q=0$ and $\sqrt{3}\times\sqrt{3}$ configurations on account of the relative size of the magnetic and nuclear cells.

Experimental studies of the nature of the magnetic ground state and excitations of kagome antiferromagnets have been hindered by difficulties in finding suitable model compounds.[11–21] One system that appears to meet the necessary criteria is the jarosite (see Fig. 3) family of minerals of general formula $AFe_3(SO_4)_2(OH)_6$, where A^+ is usually a univalent cation such as K^+ or H_3O^+,[16–21] Fe^{3+} may be exchanged for other trivalent ions such as Cr^{3+}[22,23] or V^{3+},[23] and the sulfate group may exchanged for CrO_4^{2-}.[17] In all of the iron compounds studied to date, the material behaves as a kagome array of Heisenberg $S=5/2$ spins, coupled with strong antiferromagnetic exchange. In almost all cases, long-range magnetic order is observed by neutron scattering below a temperature T_N of the order of 55 K, to produce a $q=0$ array in the *ab* plane and predominantly antiferromagnetic coupling between these planes to produce a magnetic unit cell that is

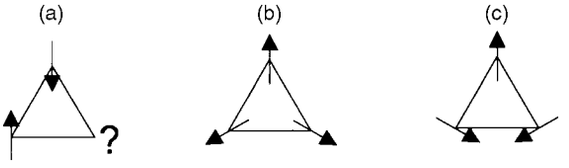

Fig. 1 Triangular plaquette of antiferromagnetically coupled moments free to rotate in the plane of the paper (a) indicates the impossibility of arranging all moments to be simultaneously antiparallel to their

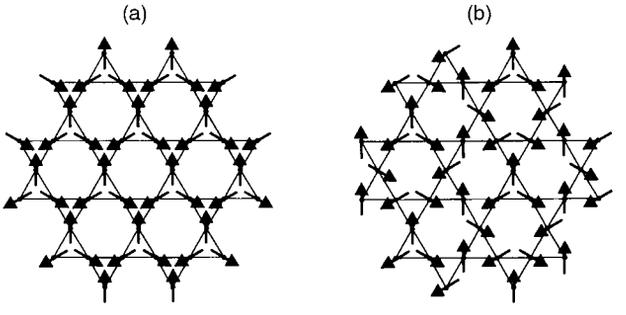

Fig. 2 Kagome lattices with (a) $q=0$ and (b) $\sqrt{3}\times\sqrt{3}$ spin arrays.

†Basis of a presentation given at Materials Discussion No. 3, 26–29 September, 2000, University of Cambridge, UK.

DOI: 10.1039/b003195j

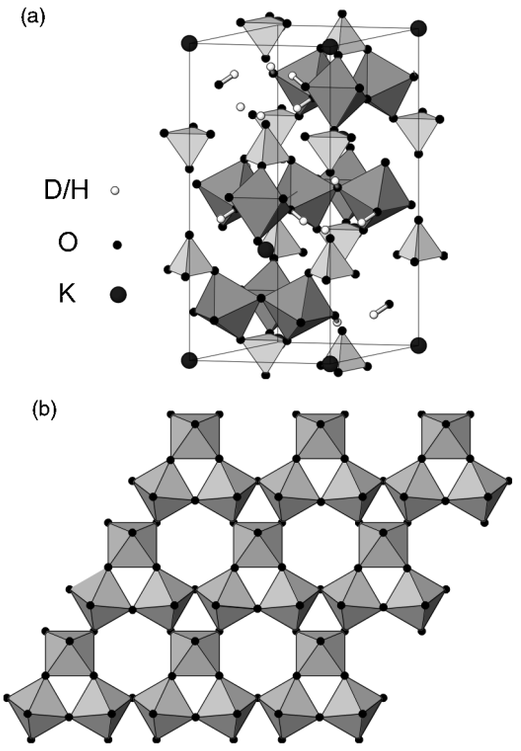

Fig. 3 (a) Crystal structure of jarosite, depicting the disposition of FeO_6 octahedra and sulfate tetrahedra and (b) detail of a single layer of Fe–O coordination octahedra viewed along the *c* axis with the iron atom at the centre of each octahedron.

doubled along the *c*-axis relative to the nuclear cell. One exception to this is the hydronium salt ($A^+ = H_3O^+$), in which the only magnetic phase change observed on cooling is a spin-glass like transition at $T_f \cong 15$ K. All the iron jarosites have essentially the same nuclear structure, but there are at least two reasons why the hydronium salt may be magnetically so different from the rest of the family: (i) the hydronium ion may provide an additional efficient pathway for inter- and intra-layer exchange *via* H-bonds, and it also has some degree of orientational disorder that may introduce a disordering influence;[3,19] (ii) the coverage of the magnetic lattice is generally higher for the hydronium salts relative to the other members of the family, which have a tendency to lose Fe from the lattice, compensating for the loss of positive charge by protonation of O–H groups elsewhere in the structure.

We investigated the second of these factors by preparing the diamagnetically-dilute deuteronium jarosite $(D_3O)Fe_{3-x}Al_y(SO_4)_2(OD)_6$ for which the occupation of the magnetic lattice was $89 \pm 3\%$. This showed a cusp in the dc magnetic susceptibility, χ_{dc}, at 25.5 K, and powder neutron diffraction data taken at 1.4 K revealed long-range magnetic order;[21,24] a similar rise in T_f on diamagnetic doping has also been observed in $(H_3O)Fe_{3-x}Ga_y(SO_4)_2(OH)_6$.[25] It is tempting therefore to suggest that in this highly frustrated magnet, diamagnetic dilution pins down a particular spin configuration from the manifold of ground states, and induces long-range magnetic order. In this paper we investigate this phenomenon further, preparing a series of diamagnetically dilute potassium jarosites, $KFe_{3-x}Al_y(SO_4)_2(OD)_6$ to follow the way in which long-range magnetic order is disturbed in this highly frustrated antiferromagnetic by diamagnetic dilution of the magnetic lattice.

2 Experimental

Samples of $KFe_{3-x}Al_y(SO_4)_2(OD)_6$ and deuterated analogues were prepared by a hydrothermal technique from anhydrous or hydrated metal sulfates as described elsewhere.[21,23] Preparations were performed at 140 ± 0.5 °C for 24 h. In all cases, the ochre coloured precipitate was washed in water (or D_2O for deuterated samples), and dried in a vacuum oven at 120 °C overnight. The percentage of aluminium and iron in the product was determined by inductively-coupled plasma atomic emission spectroscopy using a Thermo Jarrel-Ash instrument on samples that had been digested in aqua regia for 4 h and diluted with water to give a solution approximately 80 ppm in Fe^{3+}. This revealed that the samples had iron deficiencies of 5, 8 and 13% and corresponding aluminium levels of 0, 4 and 7% respectively. Thus, it appears more accurate to specify the composition of the material as $KFe_{3-x}Al_y(SO_4)_2(OD_z)_6$ (where charge neutrality is maintained by protonating the OD group such that $z-1=9-3x-3y$). However, the uncertainties in the values of elemental composition, of the order of 5%, mean that it is not possible to check that the values of *x*, *y* and *z* are precisely consistent so we will use $KFe_{3-x}Al_y(SO_4)_2(OD)_6$ or $KFe_{3-x}Al_y(SO_4)_2(OH)_6$ as the formulae for the materials through the rest of the work, and we will refer to the three deuterated materials as the $x=0.15$, 0.24 and 0.39 samples in order of decreasing iron content.

Phase purity was checked by powder X-ray diffraction on a Philips PW1730 diffractometer, with an X'Pert detection system using CuKα radiation. In all cases, no crystalline impurity phases were detected, nor was there any evidence through diffuse scattering for significant quantities of amorphous materials.

χ_{dc} was measured for each compound using a Quantum Design $MPMS_2$ SQUID magnetometer. The dependence of the magnetisation on an applied field at 5.0 K was found to be linear up to the maximum operating value of 1.0 T, and data were then taken between 1.8 and 350 K in an applied field of 1.0 T, first after cooling in zero field and then after cooling in an applied field of 1.0 T.

The nuclear structure and any magnetic correlations were studied by powder neutron diffraction on the high-flux multidetector instrument D2O at the Institut Laue Langevin (ILL) in Grenoble. Powder samples whose mass was of the order of 10 g were loaded in a vanadium can, placed in an ILL 'Orange' cryostat, and diffraction patterns taken from 2–160 K at a wavelength of 2.41(1) Å. The high flux of this instrument allowed a series of powder diffraction patterns to be measured rapidly as the sample was warmed up, producing a 'thermo-diffraction' pattern that allows phase transitions to be studied. With slightly longer counting times it is possible to take data of sufficient quality for Rietveld refinement. However, detailed analysis of the crystallographic structure is limited due to the poor resolution at high 2θ at this wavelength. Complementary measurements of any spin freezing process were made by muon spin relaxation (μSR) measurements on the spectrometer EMU at the ISIS Facility. A protonated sample of $KFe_{3-x}Al_y(SO_4)_2(OD)_6$ was prepared, analysed chemically to determine $x=0.30$ and $y=0.15$, and measurements of χ_{dc} made as for the other samples. Approximately 1 g of sample was loaded into a disc-shaped depression of 30 mm diameter cut into an aluminium plate; this was covered with mylar film to retain the sample, and the surrounding aluminium masked by a silver plate. The sample was then loaded into an Oxford Instruments 'Variox' helium cryostat, and the asymmetry in the muon decay measured from 2 to 100 K in an applied longitudinal field of 50 G (found to be sufficient to decouple the muon from the nuclear spins) to probe the nature of magnetic fluctuations above T_f, and the degree of spin freezing at lower temperatures.

3 Analysis and results

3.1 Magnetic susceptibility

All samples showed strong antiferromagnetic coupling, with Curie–Weiss behaviour above 150 K, and a maximum in χ_{dc} at a temperature T_N of the order of 50 K, falling as the coverage

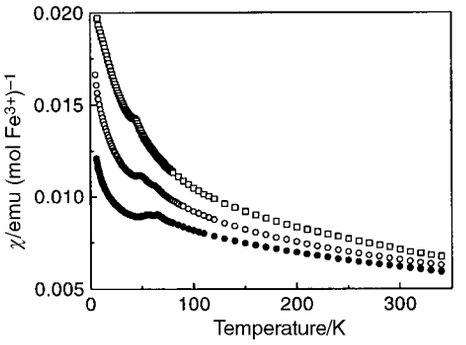

Fig. 4 Magnetic susceptibility of $KFe_{3-x}Al_y(SO_4)_2(OD)_6$ as a function of temperature measured after field-cooling in 1.0 T. Solid circles, open circles and squares refer to data with iron composition $x=0.15$, 0.24 and 0.39 respectively.

of the magnetic lattice fell (Fig. 4). Closer inspection of the maximum in χ_{dc} revealed two peaks in the samples with $x=0.15$ and 0.24, and only one distinct feature in the $x=0.39$ sample; values for the temperatures of the cusps, T_{N1} and T_{N2} for higher and lower temperature transitions respectively, are given in Table 1. The value for T_{N1} for the $x=0.39$ sample is in parentheses on account of the indistinct character of the transition, inferred from a shoulder in dI/dT from the neutron scattering data, observed to the high temperature side of the main minimum (see section 3.2). At still lower temperatures the susceptibility rose on cooling and could be fitted to a Curie–Weiss expression with a value for the Weiss constant that is considerably smaller than that at high temperature. This behaviour has been interpreted as arising from those spins nearer defects in the magnetic lattice[25] which experience on average a weaker exchange field. The data below 25 K were then fitted to a Curie–Weiss expression to produce the Curie and Weiss constants C and θ that are given in Table 1. Data taken above 150 K were then corrected for this contribution and the remaining susceptibility fitted to a Curie–Weiss expression yielding the Curie and Weiss constants C' and θ' given in Table 1. When C is expressed in emu K^{-1} mol^{-1}, it is generally taken to be approximately equal to $(\mu_{eff})^2/8$, where the effective moment $\mu_{eff}{}^2=g^2\mu_B{}^2S(S+1)$, while θ is given through the molecular field approximation by $-(4/3k)JS(S+1)$, where J is the exchange constant between a moment and the four nearest neighbours in the kagome layers.[5] Series expansion calculations[5,10] for the specific case of a Heisenberg kagome antiferromagnet show that although these relations are correct at relatively high temperatures, that is above $T\cong JS(S+1)/k$, at lower temperatures $C=(\mu_{eff})^2/9$ and $\theta=-(2/k)JS(S+1)$. For jarosites, this cross-over temperature is approximately 350 K, so we use the lower-temperature relations to deduce the values of μ_{eff} and J given in Table 1.

3.2 Powder neutron diffraction

All neutron powder diffraction patterns were similar in appearance to those observed for other pure and dilute jarosites.[17,19,21,26] At the lowest temperatures, additional

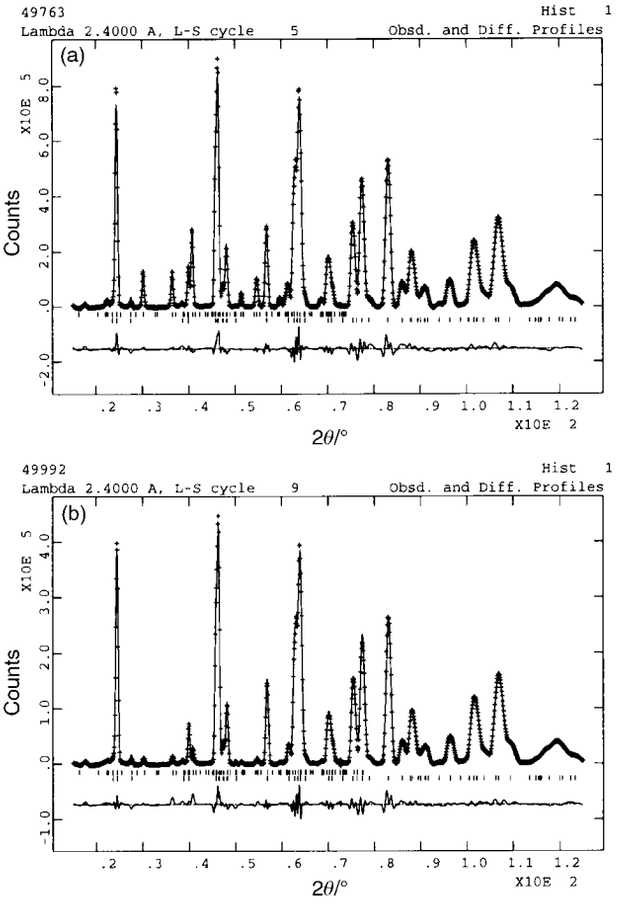

Fig. 5 Neutron diffraction data for $KFe_{3-x}Al_y(SO_4)_2(OD)_6$ with $x=0.15$ taken at (a) 18.12 K (top) and (b) 61.65 K (bottom). The line through the data represents the profile calculated after Rietveld refinement, with the difference between calculated and measured profiles given in the trace below. The upper set of tick marks indicates reflections for the magnetic scattering, while the lower set is for the nuclear scattering.

Bragg peaks appeared compared with data taken above 70 K, and these were attributed to long range magnetic order (Figs. 5–7). These peaks could be indexed on a unit cell with the same a parameter as the nuclear cell, but doubled along the c-axis, as observed for spin structures in other jarosites.[17,19,21,22,26] The evolution of the spin structure on cooling may be illustrated by integrating the intensity of a prominent magnetic peak and plotting against temperature. The top panel of Fig. 8 shows how the intensity I of the (1 1 3/2) reflection for the $x=0.15$ sample depends on temperature, while the middle panel shows the derivative of I with respect to temperature, revealing more clearly a second transition at lower temperature. The bottom panel reproduces χ_{dc} over this temperature range, mirroring the behaviour of dI/dT. The precise value of T_N derived from the temperature dependence of the intensity of a magnetic Bragg peak is generally taken as the temperature at which dI/dT is most negative; at this point the rate of decay of

Table 1 Magnetic parameters for aluminium-doped potassium jarosites with different iron contents derived from χ_{dc} and powder neutron diffraction data: T_{N1} and T_{N2} are the temperatures of the higher and lower temperature cusps in the susceptibility, C is the gradient of the inverse susceptibility plotted against temperature for the linear region above 150 K and θ is the intercept of this line with the temperature axis; μ_{eff} and J are the effective moment and exchange constant derived from C and θ respectively. C' and θ' are Curie and Weiss constants extracted from data taken below 25 K, as described in the text

Composition x of $KFe_{3-x}Al_y(SO_4)_2(OD)_6$	T_{N1}, T_{N2}/K	θ/K	C/emu mol^{-1} K^{-1}	θ'/K	C'/emu mol^{-1} K^{-1}	μ_{eff}/μ_B	J/K
0.15	64.5(0.5), 57.0(0.5)	−663(2)	5.78(1)	−6.83(12)	0.0545	6.8	37.9(1)
0.24	60.5(1.0), 45.5(1.0)	−630(5)	5.69(3)	−12.8(1)	0.14	6.74	35.0(3)
0.39	(53.5(2.0)), 41.5(1.0)	−430(19)	5.55(3)	—	—	6.66	24.6(1.1)

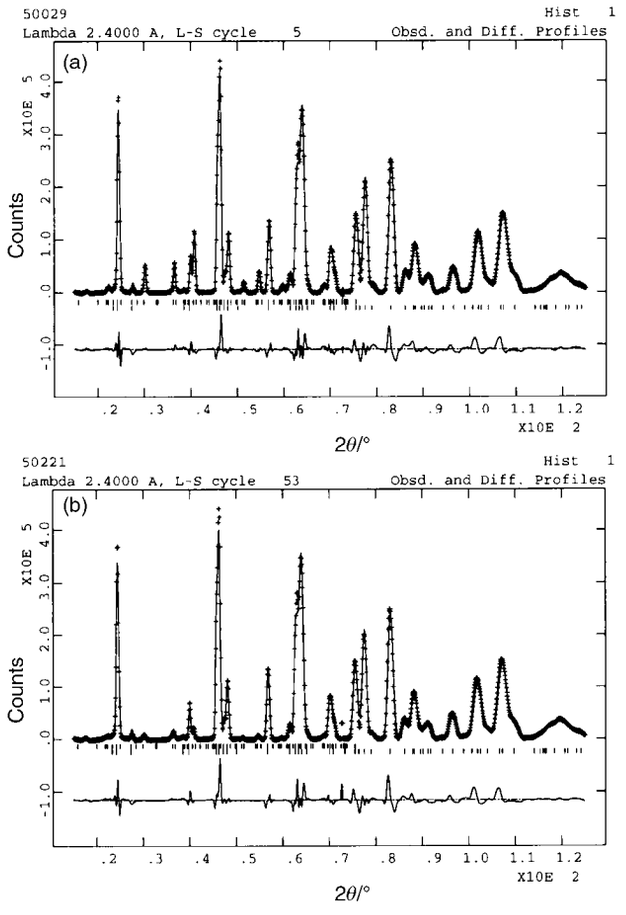

Fig. 6 Neutron diffraction data for $KFe_{3-x}Al_y(SO_4)_2(OD)_6$ with $x=0.24$ taken at (a) 18.18 K (top) and (b) 57.0 K (bottom). The line through the data represents the profile calculated after Rietveld refinement, with the difference between calculated and measured profiles given in the trace below. The upper set of tick marks indicate reflections for the magnetic scattering, while the lower set is for the nuclear scattering.

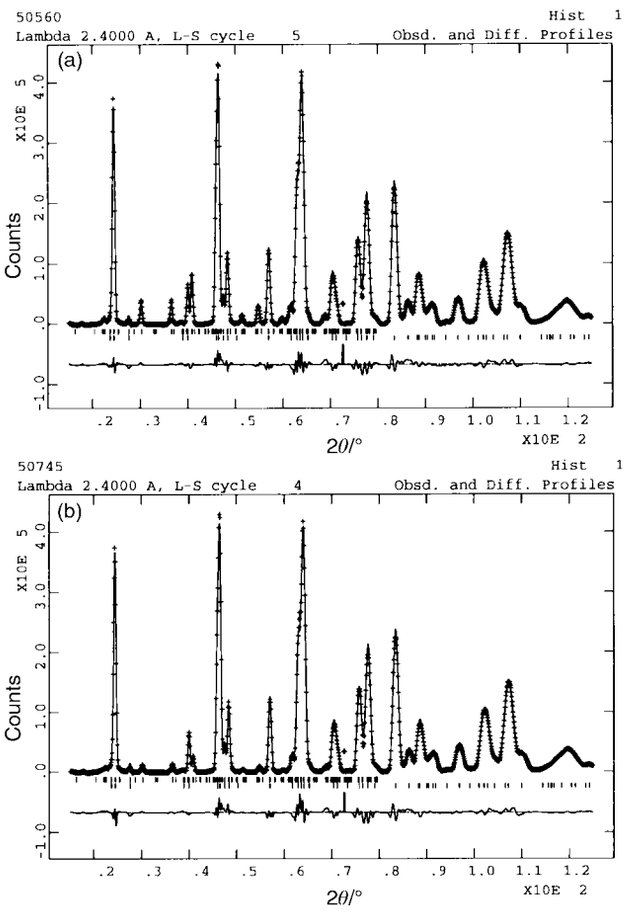

Fig. 7 Neutron diffraction data for $KFe_{3-x}Al_y(SO_4)_2(OD)_6$ with $x=0.39$ taken at (a) 6.03 K (top) and (b) 53.83 K (bottom). The line through the data represents the profile calculated after Rietveld refinement, with the difference between calculated and measured profiles given in the trace below. The upper set of tick marks indicate reflections for the magnetic scattering, while the lower set is for the nuclear scattering.

the magnetic Bragg peak is greatest, and this is compounded by a maximum in the critical scattering that arises from short-range magnetic correlations.[27] The result of this analysis applied to all three samples is summarised in Table 1, and Figs. 9 and 10 reproduce the temperature dependence of I, dI/dT and χ_{dc} for the $x=0.24$ and 0.39 samples respectively.

Diffraction patterns were selected for Rietveld refinement of the nuclear and magnetic structures for each sample at temperatures that appeared to represent each of the ordered magnetic phases. Thus, for the $x=0.15$ sample, patterns were selected at 18.12 K and at 61.65 K; for the $x=0.24$ sample at 18.18 K and 57.0 K; and for the $x=0.39$ sample at 6.03 K and 53.83 K. This last data set was not taken at an ideal temperature because a judgement of where best to take a pattern for the intermediate magnetic phase was made before careful analysis of dI/dT. Initial values for the various structural parameters were taken from refinements of other $AFe(SO_4)_2(OD)_6$ compounds, and in particular for the potassium salt,[17,26] and the refinement was performed using the program suite GSAS.[28] Structural parameters determined in this fashion are given for $KFe_{3-x}Al_y(SO_4)_2(OD)_6$ with $x=0.15$, 0.24 and 0.39 and at temperatures of 18.12, 18.18 and 6.03 K in Tables 2, 3 and 4 respectively. The magnetic structure proposed previously for potassium iron jarosite[17] can be described using a propagation vector (in the nonprimitive hexagonal cell) of $\boldsymbol{k}=(0, 0, 3/2)$. Group theory calculations using the technique of Representational Analysis[29,30] indicate that only three possible magnetic structures are compatible with this value of $\boldsymbol{k}$. A good agreement with the experimental data was achieved only with one of these values. If the atomic sites are labeled Fe1 = (0.5, 0.5, 0.5), Fe2 = (0.5, 0, 0.5) and Fe3 = (0, 0.5, 0.5) , this model corresponds to the combination of two basis vectors. With respect to the hexagonal crystallographic cell these can be written: $\boldsymbol{\Psi}_{1,Fe1}=(1\ -1\ 0)$, $\boldsymbol{\Psi}_{1,Fe2}=(1\ 2\ 0)$, $\boldsymbol{\Psi}_{1,Fe3}=(-2\ -1\ 0)$ and $\boldsymbol{\Psi}_{2,Fe1}=\boldsymbol{\Psi}_{2,Fe2}=\boldsymbol{\Psi}_{2,Fe3}=(0\ 0\ 1)$

The first basis vector corresponds to a planar 120° array of moments and the second to an array with a component along the c-axis. Any linear combination of these two basis vectors corresponds to a symmetry-allowed solution, and so in general

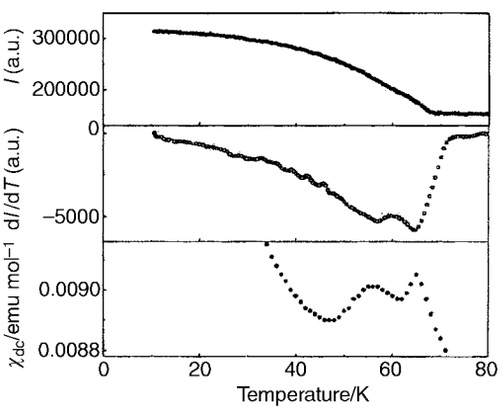

Fig. 8 Magnetic phase transitions in $KFe_{3-x}Al_y(SO_4)_2(OD)_6$ with $x=0.15$ revealed by the intensity I of the (1 1 3/2) reflection in the powder neutron diffraction pattern (top), through dI/dT for the same reflection (middle) and χ_{dc} (bottom).

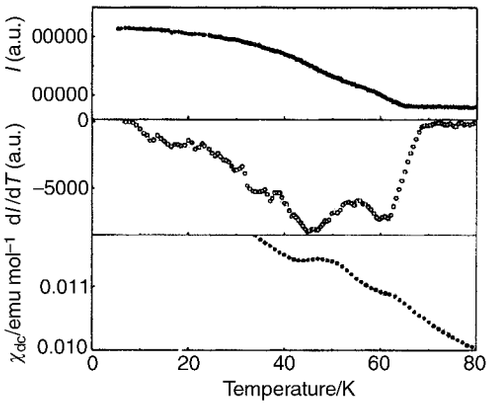

Fig. 9 Magnetic phase transitions in $KFe_{3-x}Al_y(SO_4)_2(OD)_6$ with $x=0.24$ revealed by the intensity I of the (1 1 3/2) reflection in the powder neutron diffraction pattern (top), through dI/dT for the same reflection (middle) and χ_{dc} (bottom).

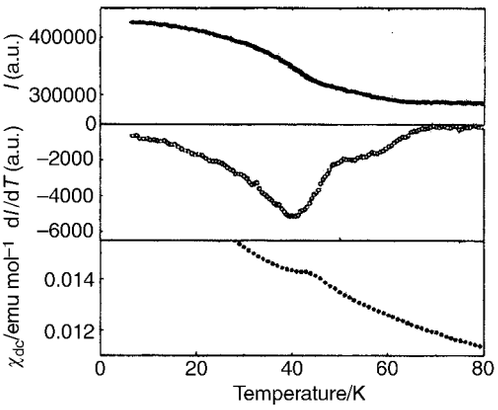

Fig. 10 Magnetic phase transitions in $KFe_{3-x}Al_y(SO_4)_2(OD)_6$ with $x=0.39$ revealed by the intensity I of the (1 1 3/2) reflection in the powder neutron diffraction pattern (top), through dI/dT for the same reflection (middle) and χ_{dc} (bottom).

the possible projections of the magnetic moment, M, are given by

$$M = C_1\Psi_1 + C_2\Psi_2$$

Refinement was made directly in terms of these basis vector mixing coefficients C_n using a reverse Monte-Carlo (RMC) algorithm in which only random changes to these coefficients that improved χ^2 were accepted. 400 such cycles were made, and these proved to be sufficient to find a fit minimum that could not be significantly improved by conventional least-squares methods. The magnetic structure factor calculations were performed using the GENLES routine of the GSAS refinement suite.[28] Representational Analysis calculations and the RMC refinement of the basis vector mixing coefficients were carried out using the package SARA*h*.[31]

Refinements are displayed in Figs. 5–7 in order of decreasing iron coverage. Optimised parameters for the magnetic structure are given in Table 5. The site occupancy of the iron atoms was also refined and found to be consistently 2% higher than the values found for chemical analysis. It should also be noted that it is difficult to make precise and meaningful comparisons between the ordered magnetic moment refined for the intermediate phases because the temperatures for which data were taken and refined correspond to different points on the respective sublattice magnetisation curves *i.e.* the reduced temperature $(T_{N1}-T)/T_{N1}$ is similar for the $x=0.15$ and $x=0.24$ samples, but quite different for the $x=0.39$ sample.

3.3 Muon spin relaxation

At relatively high temperatures ($T>70$ K), the asymmetry of the decay of the muon polarisation, $G(t)$, could be fitted well to the expression:

$$G(t) = a_0^1 \exp(-\lambda t) + a_0^2$$

The time-independent term a_0^1 arises from implantation of some of the muons in the silver part of the sample holder, while the exponential term is what is expected for muon spin depolarisation in a paramagnet, where the relaxation rate $\lambda = 1/T_1$, and a_0^1 is the initial asymmetry for this component of the depolarisation. As the sample is cooled further, a_0^1 was observed to drop in two stages, first from about 67 K and then from about 47–50 K as displayed in Fig. 11; the susceptibility of this sample measured on the SQUID magnetometer is similar to that for the deuterated $x=0.24$ sample (Figs. 4 and 9) with maxima at 47 K, and 65 K. λ shows

Table 2 Structural parameters for $KFe_{3-x}Al_y(SO_4)_2(OD)_6$ with $x=0.15$ and $y=0$ derived from Rietveld refinement of neutron powder diffraction data taken at 18.12 K in the space group $R\bar{3}m$ with $Z=3$. Figures reported without errors were not refined. Nuclear cell parameters: $a=7.24402(21)$ Å, $c=16.99335(74)$ Å; $R_{wp}=4.73\%$, $R_p=3.51\%$ (at 61.65 K: $a=7.24976(20)$ Å, $c=17.00999(66)$ Å)

Atom (Wyckoff site)	x	y	z	U_{iso}/Å^2	Site symmetry	Fractional occupancy
Fe (9d)	0.50000	0.50000	0.50000	0.0100(*)	2/M(110)	0.95
S (6c)	0.00000	0.00000	0.30774(75)	0.0219(44)	3M(100)	1.000
O1 (6c)	0.00000	0.00000	0.39068(38)	0.0058(11)	3M(100)	1.000
O2 (18h)	0.22473(22)	−0.22473(22)	−0.05425(20)	0.0058(11)	M(110)	1.000
O3 (18h)	0.12782(27)	−0.12782(27)	0.13626(26)	0.0058(11)	M(110)	1.000
K (3a)	0.00000	0.00000	0.00000	0.052(4)	−3M(100)	1.000
D4 (18h)	0.19706(22)	−0.19707(23)	0.11054(18)	0.0168(18)	M(110)	1.000

Table 3 Structural parameters for $KFe_{3-x}Al_y(SO_4)_2(OD)_6$ with $x=0.24$ derived from Rietveld refinement of neutron powder diffraction data taken at 18.2 K in the space group $R\bar{3}m$ with $Z=3$. Figures reported without errors were not refined. Nuclear cell parameters: $a=7.21044(6)$ Å, $c=16.90761(115)$ Å; $R_{wp}=5.96\%$, $R_p=4.2\%$ (at 57.0 K: $a=7.21071(7)$Å, $c=16.91207(123)$ Å)

Atom (Wyckoff site)	x	y	z	U_{iso}/Å^2	Site symmetry	Fractional occupancy
Fe (9d)	0.50000	0.50000	0.50000	0.01(*)	2/M(110)	0.92
S (6c)	0.00000	0.00000	0.30610(115)	0.0201(67)	3M(100)	1.000
O1 (6c)	0.00000	0.00000	0.38975(57)	0.0066(16)	3M(100)	1.000
O2 (18h)	0.22507(32)	−0.22507(32)	−0.05417(30)	0.0066(16)	M(110)	1.000
O3 (18h)	0.12750(40)	−0.12750(40)	0.13669(40)	0.0066(16)	M(110)	1.000
K (3a)	0.00000	0.00000	0.00000	0.052(4)	−3M(100)	1.000
D4 (18h)	0.19653(37)	−0.19653(37)	0.11046(28)	0.0220(28)	M(110)	1.000

Table 4 Structural parameters for $KFe_{3-x}Al_y(SO_4)_2(OD)_6$ with $x=0.39$ derived from Rietveld refinement of neutron powder diffraction data taken at 6.03 K in the space group $R\bar{3}m$ with $Z=3$. Figures reported without errors were not refined. Nuclear cell parameters: $a=7.21182(23)$ Å, $c=16.96039(77)$ Å; $R_{wp}=4.03\%$, $R_p=2.85\%$ (at 53.83 K: $a=7.21321(23)$ Å, $c=16.96639(77)$ Å)

Atom (Wyckoff site)	x	y	z	U_{iso}/Å^2	Site symmetry	Fractional occupancy
Fe (9d)	0.50000	0.50000	0.50000	0.0281(*)	2/M(110)	0.87
S (6c)	0.00000	0.00000	0.30707(73)	0.0201(46)	3M(100)	1.000
O1 (6c)	0.00000	0.00000	0.39197(35)	0.0690(72)	3M(100)	1.000
O2 (18h)	0.22427(20)	−0.22427(20)	−0.05430(19)	0.0690(72)	M(110)	1.000
O3 (18h)	0.12654(30)	−0.12654(30)	0.13580(30)	0.0691(72)	M(110)	1.000
K (3a)	0.00000	0.00000	0.00000	0.052 (4)	−3M(100)	1.000
D4 (18h)	0.19633(21)	−0.19633(21)	0.11113 (16)	0.0229 (17)	M(110)	1.000

relatively little change on cooling, except for a small maximum in the region of 45 K.

If the magnetic moments in the sample freeze in an ordered array, the muon polarisation will precess at a rate that depends on the magnitude of the internal field experienced at the implantation site — indeed, previous μSR studies of potassium iron jarosite[32] show such behaviour below approximately 60 K, with two principal Fourier components whose frequency saturates at approximately 21 and 38 MHz on cooling, arising from muons that experience two different static fields in the sample (though note that the data in that experiment were not taken with sufficient resolution in temperature to observe two freezing transitions). However, EMU is fed muon pulses whose width sets an upper limit of 10 MHz to observe such precession, so we might anticipate the contribution to $G(t)$ from such a signal will effectively appear as a time-independent term, centred at 1/3 of the value of a_0 for this component; if the ordered array retains some dynamic character, this signal will also decay, though previous measurements on potassium jarosite suggest that over at least the first 0.3 μs of measurements it remains constant with time.

The onset of spin-freezing may be inferred from the drop in a_0^1 for the exponential component of $G(t)$ on cooling, with transitions at 67 K, and 45–47 K, consistent with the susceptibility data. The observation of a weak maximum in λ at T_{N2} suggests that a proportion of the moments are still slowing down and freezing at this temperature — possibly because one or more components of the moments are not static in the intermediate phase on the timescale of the muon experiment. The observation that there is no such maximum at T_{N1} might simply arise when muons are implanted in sites of relatively high symmetry and the ordered array produced a null field at the muon site. This would be the case, for example, if the moments froze into triangular antiferromagnetic arrays, and the muons were implanted at sites equidistant from each moment. It should be noted that a similar maximum at T_{N2} in $1/T_1$ was observed in ^{23}Na NMR measurements on sodium iron jarosite.[26,33]

4 Discussion

Diamagnetic dilution of potassium iron jarosite leads to a reduction in the exchange field experienced by the most strongly coupled moments, and also in the magnetic freezing temperatures, exactly as might be expected when a conventional magnet is diluted. The observation of two magnetic transitions is well documented for a number of other jarosites with A cations K^+, Na^+,[18,30] Rb^+ and Ag^+,[21] but there has been no clear assignment of the states involved, and the perturbations that must be applied to the Hamiltonian for a simple nearest-neighbour kagome Heisenberg antiferromagnet to cause such behaviour. Further-neighbour exchange is known to stabilise various forms of magnetic long-range order[5,10] and Ising anistropy also causes a symmetry-breaking transition, though without long-range magnetic order.[37,38] Ising kagome antiferromagnets with further-neighbour in-plane interactions reveal complex magnetic phase diagrams, and successive phase transitions on cooling,[34–38] but the iron jarosites are not expected to represent such models well. The influence of further-neighbour exchange interactions on XY kagome antiferromagnets has also been investigated,[39] but only up to in-plane second-neighbour interactions, which induce a single transition to a long-range ordered state. It therefore appears that there is still no theoretical work for a Heisenberg kagome antiferromagnet subject to all the perturbations that are likely to be significant for jarosites, and which reproduces the magnetic phases observed for much of the family.

Our measurements, in combination with observations of ordering processes in the sodium and potassium salts[26,30] shed some light on the nature of the phases between T_{N1} and T_{N2} and below T_{N2}, and allow us to establish the tentative composition-magnetic phase diagram reproduced in Fig. 12. The low-temperature phase (C) was determined for polarised neutron scattering measurements on a single crystal of $KFe_3(SO_4)_2(OH)_6$ to be a coplanar array of moments in the *ab* plane,[40] while the intermediate phase (I) appears to have some degree of order of the moments along the *c*-axis, and is likely to retain some fluxional character according to the muon measurements. It should be noted that our analysis clearly indicates that phase I has components of the moment both along *c and* in the *ab* plane — attempts to refine the structure with moments exclusively in one direction or the other gave very poor fits. The character of the low temperature phase is thus compatible with theoretical work that predicts that a process of 'order by disorder' selects such

Table 5 Magnetic moments refined in the space group *P1* for $KFe_{3-x}Al_y(SO_4)_2(OD)_6$, where the components of the moments adopt a $q=0$ structure in the *ab* plane, and may cant out of this plane by an angle ϕ

Iron deficiency x	T/K	μ_{eff}/μ_B	Canting angle ϕ/°
0.15	18.12	3.942(32)	4.3
0.24	18.18	3.637(43)	5.7
0.39	6.03	2.995(30)	4.5
0.15	61.65	1.779(40)	14.5
0.24	57.0	1.755(82)	15.5
0.39	53.8	1.730(46)	12.0

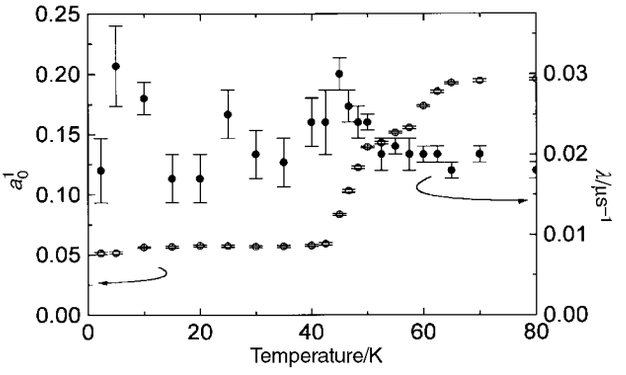

Fig. 11 Temperature dependence of the initial asymmetry, (open circles), and the relaxation rate, λ (closed circles),of the exponential component of decay of muon polarisation in $KFe_{3-x}Al_y(SO_4)_2(OD)_6$ with $x=0.30$ and $y=0.15$.

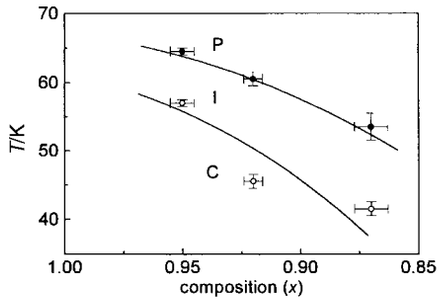

Fig. 12 Magnetic-compositional phase diagram for $KFe_{3-x}Al_y(SO_4)_2(OD)_6$ delineating the paramagnetic (P), intermediate (I) and coplanar (C) phases, where values of x are taken from chemical analysis.

coplanar states, and within experimental error this coplanarity is robust towards dilution up to at least the $x=0.39$ sample. The character of the intermediate phase is not really treated explicitly by current theory and one can only speculate that either a temperature-dependent Ising anisotropy, or the influence of thermal fluctuations, may tip the moments out of the *ab* plane before the system becomes paramagnetic.

The ordered moment in all of the samples at the lowest temperatures is significantly smaller than would be expected on the basis of the electronic configuration of Fe^{3+} in these materials. This may be due in part to a component of the scattering residing in the diffuse background, as has been observed in a full three-directional (*xyz*) polarised neutron study of $KFe_3(SO_4)_2(OD)_6$.[41] However, that study also revealed that the total integrated static structure factor at 1.5 K was smaller than expected, suggesting that even at this low temperature there are fluctuations faster than the time-scale of this neutron experiment (10^{-11}–10^{-13} s); this conclusion is compatible with the observation that in the related $S=3/2$ system, less than 50% of the sublattice magnetisation is observed in neutron scattering measurements at $T\approx 0$.[22]

5 Conclusions

It is clear from this and other work on the composition and magnetic properties of jarosites that it is difficult to produce materials with consistent and controlled coverage of the magnetic lattice. T_{N1} and T_{N2} for potassium iron jarosite are reduced on dilution of the iron sublattice, along with the average exchange field, which is consistent with the behaviour anticipated for a conventional magnet. The observation that long-range order is observed in potassium iron jarosite with at least 95% coverage of the magnetic lattice suggests that the difference between the jarosites that show long-range magnetic order, and the hydronium salts which have similar coverages and show spin-glass order, lies in other factors. Hydronium salts may provide a different form of further-neighbour inter- and/or intra-plane exchange, and perhaps also a random element through its structural disorder, and such influences will be amplified through the sensitivity of this system to small perturbations in the Hamiltonian. There is clearly a need to study a wider range of perturbed model systems, exploring the influence of 2nd and 3rd nearest neighbour in-plane exchange, as well as interlayer exchange, together with Ising or XY anisotropy, all of which may be significant in jarosites and lead to the more complex phase behaviour observed. Finally, detailed single-crystal polarised neutron studies of the intermediate phase are required to complement data taken in the low-temperature phase.

Acknowledgements

The authors are grateful to the EPSRC for financial support, and to both The ISIS Facility at the Rutherford Laboratory and also to the Institut Laue-Langevin for technical support and hospitality. A.H. is also grateful to the Nuffield Foundation, and D.V. thanks NWO (The Netherlands) for further financial aid. A.S.W. thanks the TMR project of the EC for his support, together with the Canadian Institute for Neutron Scattering and to the Royal Society of Chemistry for further support while some of this work was being conducted.

References

1 P. W. Anderson, *Science*, 1987, **235**, 1196.
2 A. P. Ramirez, *Ann. Rev. Mater. Sci.*, 1994, **24**, 453.
3 A. P. Ramirez, *Handbook of Magnetism*, vol. 6 of *Magnetic Materials*, ed. K. Buschow, Elsevier, Amsterdam, 2000, in press.
4 P. Chandra and P. Coleman, *Phys. Rev. Lett.*, 1991, **66**, 100.
5 A. B. Harris, C. Kallin and A. J. Berlinsky, *Phys. Rev. B*, 1992, **45**, 2899.
6 J. T. Chalker, P. C. W. Holdsworth and E. F. Shender, *Phys. Rev. Lett.*, 1992, **65**, 855.
7 A. Chubukov, *Phys. Rev. Lett.*, 1992, **69**, 832.
8 S. Sachdev, *Phys. Rev. B*, 1992, **45**, 12377.
9 E. F. Shender, V. B. Cherepanov, P. C. W. Holdsworth and A. J. Berlinsky, *Phys. Rev. Lett.*, 1993, **70**, 3812.
10 J. N. Reimers and A. J. Berlinsky, *Phys. Rev. B*, 1993, **48**, 9539.
11 A. P. Ramirez, G. P. Espinosa and A. S. Cooper, *Phys. Rev. Lett.*, 1990, **64**, 2070.
12 C. Broholm, G. Aeppli, G. P. Espinosa and A. S. Cooper, *Phys. Rev. Lett.*, 1990, **65**, 3173.
13 B. Martinez, F. Sandiumenge, A. Rouco, A. Labarta, J. Rodríguez-Carvajal, M. Tovar, M. T. Causa, S. Galí and X. Obradors, *Phys. Rev. B*, 1992, **46**, 10786.
14 Y. J. Uemura, A. Keren, K. Kojima, L. P. Le, G. M. Luke, W. D. Wu, Y. Ajiro, T. Asano, Y. Kuriyama, M. Mekata, H. Kikuchi and K. Kakurai, *Phys. Rev. Lett.*, 1994, **73**, 3306.
15 A. P. Ramirez, B. Hessen and M. Winkelmann, *Phys. Rev. Lett.*, 2000, **84**, 2957.
16 N. Wada, T. Kobayashi, H. Yano, T. Okuno, A. Yamaguchi and K. Awaga, *J. Phys. Soc. Jpn.*, 1997, **66**, 961.
17 M. G. Townsend, G. Longworth and E. Roudaut, *Phys. Rev. B*, 1986, **33**, 49129.
18 S. Maegawa, M. Nishiyama, N. Tanaka, A. Oyamada and M. Takano, *J. Phys. Soc. Jpn.*, 1996, **65**, 2776.
19 A. S. Wills and A. Harrison, *J. Chem. Soc., Faraday Trans*, 1996, **92**, 2161.
20 A. S. Wills, A. Harrison, S. A. M. Mentink, T. E. Mason and Z. Tun, *Europhys. Lett.*, 1998, **42**, 325.
21 A. S. Wills, A. Harrison, C. Ritter and R. I. Smith, *Phys. Rev. B*, 2000, **61**, 6157.
22 S.-H. Lee, C. Broholm, M. F. Collins, L. Heller, A. P. Ramirez, Ch. Kloc, E. Bucher, R. W. Erwin and N. Lacevic, *Phys. Rev. B.*, 1997, **56**, 8091.
23 A. S. Wills, PhD Thesis, The University of Edinburgh, 1997.
24 A. Harrison, A. S. Wills and C. Ritter, *Physica B*, 1998, **241–243**, 722.
25 S. A. Earle, A. P. Ramirez and R. J. Cava, *Physica B*, 1999, **262**, 199.
26 T. Inami, S. Maegawa and M. Takano, *J. Magn. Magn. Mater.*, 1998, **177**, 752.
27 M. F. Collins, *Magnetic Critical Scattering*, Oxford University Press, Oxford, 1989.
28 A. C. Larson and R. B. Von Dreele, *General Structure Analysis System*, 1995.
29 E. F. Bertaut, *Acta Crystallogr., Sect. A*, 1968, **24**, 217.
30 E. F. Bertaut, *J. Phys. Colloq.*, 1971, **1**, 462.
31 A. S. Wills, *Physica B*, 2000, **276–278**, 680.
32 A. Keren, K. Kojima, L. P. Le, G. M. Luke, W. D. Wu, Y. J. Uemura, M. Takano, H. Dabkowska and M. J. P. Gingras, *Phys. Rev. B*, 1996, **53**, 6451.
33 S. Maegawa and M. Nishiyama, personal communication, 1997.
34 A. Kuroda and S. Miyashita, *J. Phys. Soc. Jpn.*, 1995, **64**, 4509.
35 S. T. Bramwell and M. J. P. Gingras private communication, 1994.
36 P. Azaria, H. T. Diep and H. Giacomini, *Phys. Rev. Lett.*, 1987, **59**, 1629.
37 M. Wolf and K. D. Schotte, *J. Phys. A*, 1988, **21**, 2195.
38 T. Tagaki and M. Mekata, *J. Phys. Soc. Jpn.*, 1993, **62**, 3943.
39 R. S. Gekht and I. N. Bondarenko, *JETP*, 1998, **86**, 1209.
40 E. Lelievre-Berna, A. Harrison, G. S. Oakley and D. Visser, *Annual Report of the Institut Laue-Langevin for 1999*, 2000, experiment 5-61-37.
41 G. S. Oakley, D. Visser, J. Frunzke, K. H. Andersen, A. S. Wills and A. Harrison, *Physica B*, 1999, **267–268**, 142.